Observation of the dynamical structure arising from spatially extended quantum entanglement and long-lived quantum coherence in the KHCO$_3$ crystal

François Fillaux*

LADIR-CNRS, UMR 7075 Université P. et M. Curie, 2 rue Henry Dunant, 94320 Thiais, France

Alain Cousson

Laboratoire Léon Brillouin (CEA-CNRS), C.E. Saclay, 91191 Gif-sur-Yvette cedex, France

David Keen

ISIS Facility, Rutherford Appleton Laboratory, Chilton, Didcot, OX11 0QX, United Kingdom
and Physics Department, Oxford University, Clarendon Laboratory, Parks Road, Oxford OX1 3PU, United Kingdom

The crystal structures of KHCO$_3$ and KDCO$_3$ at 14 K were determined with the single-crystal neutron-diffraction technique. There is no evidence for proton/deuteron disorder. The diffraction pattern of KHCO$_3$ reveals rods of intensity separate from the Bragg peaks. These rods are not observed for KDCO$_3$. They are attributed to diffraction by the sublattice of protons forming regular arrays of double slits parallel to the dimer planes. They reveal quantum coherence in two dimensions for the proton dynamics. It is shown that quantum statistics for fermions impose quantum entanglement and strict separation of the H dynamics from the lattice. The main decoherence mechanism for the vibrational states is thus canceled out. The vibrational ground state is a superposition of fully entangled macroscopic wave functions with long-lived quantum coherence.

I. INTRODUCTION

The nonlocal nature of quantum entanglement has remained a subject of great interest since the earliest days of quantum mechanics as it causes many of the paradoxes and lies at the heart of the profound difference between quantum mechanics and classical physics.[1–5] Quantum entanglement is observed primarily for simple quantum objects (photons or/and atoms) in environments specially designed to minimize quantum decoherence and dissipation.[6–10]

Quantum entanglement is also intrinsic to a broad class of condensed systems and gives rise to short-lived and spatially restricted coherent dissipative structures.[11,12] For example, quantum entanglement on a very short time scale ($<10^{-15}$ s) has been evidenced for protons with the neutron Compton scattering technique.[13–16]

In a complex system, an initially entangled subsystem loses its ability to exhibit quantum interference by getting entangled with the ambient degrees of freedom, via interaction with the surrounding environment.[17,18] This decoherence mechanism is inherent to measurements with classic apparatus and the validity of quantum mechanics at the macroscopic level is still an open question.[19] However, the exotic behavior of superconductivity and superfluidity, along with that of laser light, are manifestations of macroscopic quantum effects. Therefore it has been conjectured that a macroscopic system with many microscopic degrees of freedom can behave quantum mechanically if it is suitably decoupled from its environment.[20] This is in line with experimental demonstrations of the superposition of distinct macroscopic current states in superconducting quantum interference devices (SQUID's).[21] Similarly, vibrational spectroscopy techniques demonstrate macroscopic quantum coherence in the crystalline state, up to room temperature, for the interconver-

sion of benzoic acid dimers, via quantum proton transfer.[22]

An ideal situation to observing long-lived quantum entanglement is realized when perfect shielding from the environment occurs naturally. This can be the case for protons in the crystalline state when the separation of the proton dynamics from the crystal lattice is an inviolable consequence of the Pauli principle.[23] Then, decoherence is forbidden by the very nature of the crystal and this "intrinsic" shielding is not limited by experimental or technical feats.

Quantum interference arising from such long-lived quantum entanglement of protons have been reported for the crystal of potassium hydrogen carbonate (KHCO$_3$, see Fig. 1).[24] In this system all protons are crystallographically equivalent
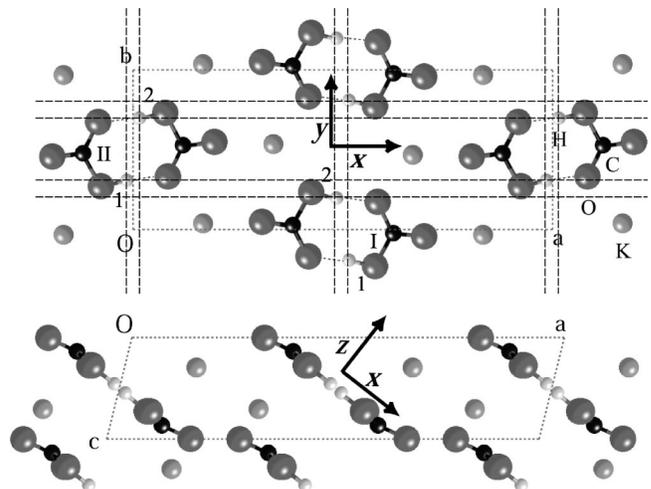

FIG. 1. Schematic view of the crystalline structure of KHCO$_3$ at 14 K. The dotted lines represent the unit cell. The dashed lines joining protons are guides for the eye (see text).

and indistinguishable. The crystal is composed of centrosymmetric dimers $(HCO_3^-)_2$ linked by hydrogen bonds. The local dynamics of protons can be represented with symmetric pairs of coupled oscillators. In the degenerate ground state, the Pauli principle imposes antisymmetrization of the vibrational wave function with respect to permutation of the indistinguishable fermions and strict separation of the proton dynamics from other atoms. The resulting proton spin correlation was probed with the elastic neutron-scattering technique and quantum interference was observed.

In these experiments quantum entanglement was probed on a spatial scale, on the order of the unit-cell dimensions, corresponding to the coherence length of ≈ 20 Å of the incident neutron beam.[25] However, some observations suggest that quantum correlation could occur on a much larger scale. In order to substantiate these preliminary results, we have performed neutron-diffraction experiments at a low temperature with much greater coherence lengths. Neutrons diffracted by the sublattice of entangled protons give rods of intensity observed in between the Bragg peaks. This is direct evidence for the dynamical structure due to quantum correlation in two dimensions. There is no such evidence of quantum entanglement for the deuterated analog $KDCO_3$, in accordance with the different quantum statistics for H and D atoms.

In Sec. II, we present the structures of $KHCO_3$ and $KDCO_3$ at 14 K determined with the single-crystal neutron-diffraction technique. The theoretical model for quantum entanglement is presented in Sec. III. In Sec. IV, we examine a rather large volume of the reciprocal space measured with the time-of-flight neutron-diffraction technique. It is shown that the ridges of intensity observed in between the Bragg-peaks for $KHCO_3$ have all the characteristics anticipated for coherent scattering by the sublattice of entangled protons in two dimensions.

II. CRYSTAL STRUCTURE

Single crystals of $KHCO_3$ and $KDCO_3$ were obtained by slow recrystallization from aqueous solutions in H_2O and D_2O, respectively. For neutron-diffraction measurements, approximately cubic samples ($3 \times 3 \times 3$ mm^3) were cut from large crystals and tested at room temperature. Each sample was loaded into an aluminum container that was mounted in a cryostat and then cooled down with a flow of helium vapor. Measurements (see Table I) were carried out on a Stoe four-circle diffractometer 5C2 at the Orphée reactor (Laboratoire Léon-Brillouin).[26]

The structure is similar to those previously reported at higher temperatures.[27,28] The crystal is monoclinic, space group $P2_1/a$ (C_{2h}^5), with four $KHCO_3$ ($KDCO_3$) entities per unit cell (Fig. 1 and Tables II–IV). The carbonate moieties, linked by hydrogen (deuterium) bonds with length O $\cdots$O$\approx 2.587(1)$ Å [$2.607(1)$ Å for $KDCO_3$], form quasiplanar centrosymmetric dimer entities $(HCO_3^-)_2$ and $(DCO_3^-)_2$, respectively. The dimers at C_i sites are parallel to the $(\bar{3}01)$ planes at $\approx 42°$ with respect to the (a,b) planes. All protons (deuterons) are equivalent. Whereas previous diffraction

TABLE I. Neutron single-crystal diffraction data and structure refinement for potassium hydrogen carbonate and its deuterated analog at 14 K. $\lambda = 0.8305$ Å, space group $P2_1/a$. The variance for the last digit is given in parentheses.

	KHCO$_3$	KDCO$_3$
a (Å)	15.06(2)	15.08(2)
b (Å)	5.570(15)	5.594(8)
c (Å)	3.650(8)	3.658(7)
α	90°	90°
β	103.97(15)°	103.78(15)°
γ	90°	90°
Volume	297.1(13)	299.7(9)
Reflections measured	1857	1820
Independent reflections	979	1101
Reflections used	904	967
σ(I) limit	3.00	3.00
Refinement on F		
R factor	0.026	0.040
Weighted R factor	0.020	0.039
Number of parameters	56	57
Goodness of fit	1.070	0.948
Extinction	4039.9(755)	8.8(4)

studies performed at 298 and 98 K have revealed proton disorder between two sites located at $\approx \pm 0.3$ Å off-center of the hydrogen bond, there is no visible proton disorder at 14 K (see Table II). The same conclusion applies to the deuterated derivative. The refined occupancy of 0.903(6) for the D atom in Table II arises from imperfect deuteration. It is thus confirmed that the disorder is dynamical in nature. It is governed by an asymmetric double well potential for proton (deuteron) transfer along the hydrogen bond.[29]

The thermal factor U_{33} for H atoms in Table IV compares to the mean-square displacements in the ground state of a harmonic proton oscillator corresponding to the out-of-plane bending mode observed at 960 cm^{-1} $(u_\gamma^2 \approx 1.75 \times 10^{-2}$ Å$^2)$.[24] The values for U_{22} and U_{11} are much greater than anticipated for the in-plane bending mode observed at 1360 cm^{-1} $(u_\delta^2 \approx 1.23 \times 10^{-2}$ Å$^2)$ and for the stretching mode observed at ≈ 2800 cm^{-1} $(u_\nu^2 \approx 0.60 \times 10^{-2}$ Å$^2)$. The analysis of the rigid body motion[30] performed on $(HCO_3^-)_2$ dimers (Fig. 2) gave a R factor for the temperature factors of 0.53. This value was decreased to 0.08 after removal of the H atoms. The R factor is further decreased to 0.02 for a single CO_3^{2-} entity. It transpires that proton displacements are virtually uncorrelated to CO_3^{2-} and $(CO_3^{2-})_2$ entities that can be regarded as almost perfectly rigid bodies.

III. PROTON DYNAMICS AND QUANTUM ENTANGLEMENT

Vibrational spectra of $KHCO_3$ and $KDCO_3$ have been thoroughly investigated with optical and neutron-scattering techniques.[24,29,31–35] The OH (OD) bonds are virtually parallel to each other throughout the crystal and the proton modes in the ground state are parallel to the principal axes of the

TABLE II. Atomic positions, isotropic temperature factors, and site occupancies for $KHCO_3$ (first lines), and $KDCO_3$ (second lines) at 14 K. The variance for the last digit is given in parentheses.

Atom	x/a	y/b	z/c	U(iso)(Å^2)	Occupancy
K(1)	0.166 06(2)	0.034 50(6)	0.29 48(1)	0.0043	1.000
	0.165 96(6)	0.035 92(16)	0.29 54(3)	0.0023	1.000
C(1)	0.119 525(14)	0.524 60(4)	0.854 77(6)	0.0038	1.000
	0.119 72(3)	0.525 88(9)	0.855 59(18)	0.0023	1.000
O(1)	0.193 385(17)	0.545 57(4)	0.095 81(7)	0.0056	1.000
	0.193 55(4)	0.547 46(11)	0.0962(2)	0.0040	1.000
O(2)	0.082 833(16)	0.329 36(4)	0.724 87(7)	0.0054	1.000
	0.083 16(4)	0.330 83(11)	0.7262(2)	0.0036	1.000
O(3)	0.076 310(17)	0.730 64(5)	0.724 50(7)	0.0055	1.000
	0.076 34(4)	0.731 88(11)	0.7250(2)	0.0039	1.000
H(1)	0.014 95(4)	0.694 27(9)	0.547 01(14)	0.0163	1.000
D(1)	0.015 84(5)	0.695 04(13)	0.5499(3)	0.0098	0.903(6)

dimers. In Fig. 1, these directions are schematically shown as x for stretching (ν OH/OD), y for in-plane bending (δ OH/OD) and z for out-of-plane bending (γ OH/OD). As intradimer coupling terms are much greater than interdimer analogs, the proton dynamics can be represented with isolated pairs of coupled harmonic proton oscillators along the three directions $\alpha = x, y,$ or z.[23,24] Interdimer coupling terms can be regarded as weak perturbation giving rise to phonons with small dispersion.

A. Isolated dimer

The Hamiltonian for a coupled pair of anisotropic harmonic oscillators can be written as[23,36]

$$H = \sum_\alpha H_\alpha, \alpha = x, y, \text{ or } z \text{ and}$$

$$H_\alpha = \frac{1}{2m}(P_{1\alpha}^2 + P_{2\alpha}^2) + \frac{1}{2}m\omega_{0\alpha}^2[(\alpha_1 - \alpha_0)^2 + (\alpha_2 + \alpha_0)^2 + 2\lambda_\alpha(\alpha_1 - \alpha_2)^2]. \quad (1)$$

$P_{1\alpha}$ and $P_{2\alpha}$ are the kinetic momenta. The coordinates α_1 and α_2 are the projections onto the α direction of the proton positions with respect to the projection of the dimer center of symmetry. The harmonic frequency of the uncoupled oscil-

TABLE III. Interatomic distances in Å units and angles in degrees in $KHCO_3$ (first lines) and $KDCO_3$ (second lines) at 14 K. The variance for the last digit is given in parentheses.

C(1)-O(1)	1.2460(3)	O(1)-C(1)-O(2)	125.63(2)	
	1.250(3)		125.71(6)	
C(1)-O(2)	1.2595(3)	O(1)-C(1)-O(3)	116.23(2)	
	1.2626(17)		116.14(6)	
C(1)-O(3)	1.3481(3)	O(2)-C(1)-O(3)	118.15(2)	
	1.3547(18)		118.15(13)	
O(3)-H(1)	1.0127(5)	C(1)-O(3)-H(1)	110.10(3)	
O(3)-D(1)	1.003(2)	C(1)-O(3)-D(1)	109.86(17)	

lators at equilibrium positions $\pm\alpha_0$ is $\hbar\omega_{0\alpha}$. The coupling potential proportional to λ_α depends only on the distance between the particles. The equilibrium positions of the coupled oscillators are at $\pm\alpha_0' = \pm\alpha_0/(1 + 4\lambda_\alpha)$.

With normal coordinates corresponding to symmetric and antisymmetric displacements of the particles, such as

$$\alpha_s = \frac{1}{\sqrt{2}}(\alpha_1 - \alpha_2), \ P_{\alpha s} = \frac{1}{\sqrt{2}}(P_{\alpha 1} - P_{\alpha 2}),$$

$$\alpha_a = \frac{1}{\sqrt{2}}(\alpha_1 + \alpha_2), \ P_{\alpha a} = \frac{1}{\sqrt{2}}(P_{\alpha 1} + P_{\alpha 2}), \quad (2)$$

the Hamiltonian splits into two harmonic oscillators at frequencies $\hbar\omega_{s\alpha} = \hbar\omega_{0\alpha}\sqrt{1 + 4\lambda_\alpha}$ and $\hbar\omega_{a\alpha} = \hbar\omega_{0\alpha}$, respectively.

The quantization of this system is not trivial because the two particles are indistinguishable. For bosons (for example, deuterium atoms) the wave function and energy levels can be written as

$$\Psi_{n_a n_s} = \Psi_{n_a}(\alpha_a)\Psi_{n_s}(\alpha_s - \sqrt{2}\alpha_0'),$$

$$E_{n_a n_s} = \left(n_a + \frac{1}{2}\right)\hbar\omega_{a\alpha} + \left(n_s + \frac{1}{2}\right)\hbar\omega_{s\alpha}. \quad (3)$$

The elastic scattering function is then[23]

$$S_{0\alpha}(Q_\alpha, \omega) = 2\exp\left[-Q_\alpha^2\left(\frac{u_{0\alpha}^2}{2\sqrt{1 + 4\lambda_\alpha}} + \frac{u_{0\alpha}^2}{2}\right)\right]\delta(\omega), \quad (4)$$

where $u_{0\alpha}^2 = \hbar/(2m\omega_{0\alpha})$ is the mean-square amplitude in the ground state for the uncoupled harmonic oscillators. Q_α is the projection onto α of the momentum transfer vector $\mathbf{Q} = \mathbf{k_0} - \mathbf{k_f}$ with $|\mathbf{k_0}| = 2\pi/\lambda_0$ and $|\mathbf{k_f}| = 2\pi/\lambda_f$, where λ_0 and λ_f are the incident and scattered wavelengths, respectively. The neutron energy transfer is $\hbar\omega$.

For fermions (for example protons), the wave function must be antisymmetrized with respect to particle permutation, according to the Pauli principle. Consequently, nuclear spins are correlated to the symmetry of the normal modes.

TABLE IV. Thermal parameters in Å^2 units for KHCO$_3$ (first lines) and KDCO$_3$ (second lines) at 14 K. The variance for the last digit is given in parentheses.

Atom	U$_{11}$	U$_{22}$	U$_{33}$	U$_{23}$	U$_{13}$	U$_{12}$
K(1)	0.004 64(18)	0.005 35(18)	0.002 85(16)	0.0001(1)	0.000 63(12)	−0.0000(1)
	0.0021(3)	0.0021(3)	0.0026(4)	0.0002(3)	0.0005(3)	−0.0002(2)
C(1)	0.003 46(12)	0.004 17(11)	0.003 59(11)	0.000 02(6)	0.000 79(7)	−0.000 14(6)
	0.001 77(19)	0.0018(2)	0.0033(2)	−0.000 32(17)	0.000 67(15)	−0.000 36(13)
O(1)	0.004 13(12)	0.006 72(13)	0.005 19(12)	−0.000 13(7)	−0.000 43(8)	−0.000 10(7)
	0.0025(2)	0.0039(2)	0.0050(3)	−0.0008(2)	−0.000 27(18)	−0.000 28(17)
O(2)	0.005 14(12)	0.004 28(13)	0.005 93(12)	−0.000 48(7)	−0.000 14(8)	−0.000 06(7)
	0.0031(2)	0.0016(2)	0.0051(3)	−0.000 28(18)	−0.000 75(17)	−0.000 29(16)
O(3)	0.005 31(12)	0.004 54(13)	0.005 83(13)	0.000 20(7)	−0.000 15(9)	0.000 34(7)
	0.0032(2)	0.0022(2)	0.0056(3)	0.0003(2)	−0.000 09(18)	0.000 33(16)
H(1)	0.0136(2)	0.0153(2)	0.0174(2)	0.000 43(14)	−0.001 08(16)	−0.000 09(14)
D(1)	0.0078(3)	0.0089(3)	0.0111(4)	0.0006(3)	−0.0010(2)	0.0006(2)

The ground state is a superposition of a singlet state with antiparallel spins ($S=0$) and a triplet state with parallel spins ($S=1$). For the former, the spatial part of the wave function ($\Theta_{\alpha 0+}$) is symmetrical with respect to particle permutation (Ag symmetry in the case of KHCO$_3$) and it is antisymmetrical for the triplet state ($\Theta_{\alpha 0-}$ with Au symmetry). This can be written as[23]

$$\Theta_{\alpha 0\pm}(\alpha_1,\alpha_2)$$
$$=\frac{1}{\sqrt{2}}\Psi_0^a(\alpha_a)[\Psi_0^s(\alpha_s-\sqrt{2}\alpha_0')\pm\Psi_0^s(\alpha_s+\sqrt{2}\alpha_0')]. \quad (5)$$

The singlet $|0+\rangle$ and triplet $|0-\rangle$ states resemble para and ortho species of the hydrogen molecule. For the neutron-scattering technique, this is a reference example of quantum interference arising from exchange interaction.[37] However, for free molecules, translational degrees of freedom, analogous to the antisymmetric coordinates in Eq. (2), are unbound. Therefore vibrational dynamics in the ground state are totally represented with symmetric coordinates that are invariant upon particle permutation. There is no superposition of the singlet and triplet state and the system is a mixture of the two species with well defined concentrations. The particle positions are distinguishable and quantum interferences arise because the nuclear spins are entangled. An important consequence for elastic-scattering measurements is that there is no incoherent scattering and the intensity is proportional to the total cross section for hydrogen atoms.[37]
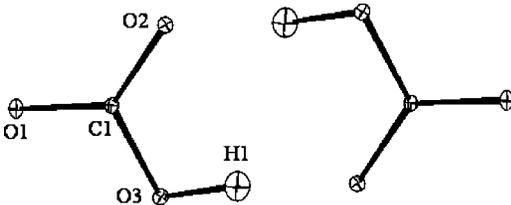

FIG. 2. Schematic view of the shape of the refined thermal ellipsoids around the atom positions for the molecular dimer (HCO$_3^-$)$_2$ at 14 K.

In the present case of two coupled oscillators, the singlet and triplet states do not correspond to different entities and quantum interference arises because both spins and positions of the two particles are entangled. The scattering function can be written as[23]

$$S(Q_\alpha,\omega)=\{|\langle\Theta_{\alpha 0\tau_i}|\exp iQ_\alpha(\alpha_1-\alpha_0')(\tau_i\tau_f)$$
$$\times\exp iQ_\alpha(\alpha_1+\alpha_0')|\Theta_{\alpha 0\tau_f}\rangle|^2$$
$$+|\langle\Theta_{\alpha 0\tau_i}|\exp iQ_\alpha(\alpha_2-\alpha_0')$$
$$\times(\tau_i\tau_f)\exp iQ_\alpha(\alpha_2+\alpha_0')|\Theta_{\alpha 0\tau_f}\rangle|^2\}\delta(\omega). \quad (6)$$

Indexes i and f refer to the initial and final states. $\tau=$ "+" or "−" for the singlet and triplet states, respectively. $(\tau_i\tau_f)$ $=$ "+" if $\tau_i=\tau_f$ or "−" if $\tau_i\neq\tau_f$. The first term of the sum corresponds to scattering by particle 1 at site 1 or site 2. The second term describes the same process for particle 2. Straightforward calculation gives[23]

$$S(Q_\alpha,\omega)_{0+0+}=\cos^2(Q_\alpha\alpha_0')\left[\cos(Q_\alpha\alpha_0')\right.$$
$$\left.+\exp\left(-\frac{\alpha_0'^2}{2u_{0\alpha}^2}\right)\right]^2 S_{0\alpha}(Q_\alpha,\omega),$$

$$S(Q_\alpha,\omega)_{0\pm0\mp}=\sin^4(Q_\alpha\alpha_0')S_{0\alpha}(Q_\alpha,\omega),$$

$$S(Q_\alpha,\omega)_{0-0-}=\cos^2(Q_\alpha\alpha_0')\left[\cos(Q_\alpha\alpha_0')\right.$$
$$\left.-\exp\left(-\frac{\alpha_0'^2}{2u_{0\alpha}^2}\right)\right]^2 S_{0\alpha}(Q_\alpha,\omega). \quad (7)$$

For the dimer of KHCO$_3$, $\alpha_0'^2\gg u_{0\alpha}^2$. The term $\exp[-\alpha_0'^2/(2u_{0\alpha}^2)]$ is negligibly small and the Gaussian-like profile, analogous to that in Eq. (4), is modulated by $\cos^4(Q_\alpha\alpha_0')$ for $|0\pm\rangle\to|0\pm\rangle$ transitions, or by $\sin^4(Q_\alpha\alpha_0')$ for $|0\pm\rangle\to|0\mp\rangle$ transitions. In ordinary counterintuitive words, these

terms arise because neutrons are scattered simultaneously by the two particles, each particle being simultaneously at both sites.

Tunneling of a single particle in a symmetric double potential is also a reference example of quantum interference for neutron scattering. Even if there is no such symmetrical double minimum potential for $KHCO_3$,[29] this case deserves particular attention for further comparison with Eq. (7). For two wells located at $\pm \alpha_0$, the scattering function for the tunneling states $|0+\rangle$ (symmetrical) and $|0-\rangle$ (antisymmetrical) can be written as[23]

$$S(Q_\alpha, \omega)_{0+0+} = \frac{1}{1+\exp\left(-\dfrac{\alpha_0^2}{2u_{0\alpha}^2}\right)} \left|\left[\cos(Q_\alpha \alpha_0)\right.\right.$$
$$\left.\left.+\exp\left(-\dfrac{\alpha_0^2}{2u_{0\alpha}^2}\right)\right]\right|^2 \bar{S}(Q_\alpha)\delta(\omega),$$

$$S(Q_\alpha, \omega)_{0\pm 0\mp} = \frac{1}{\sqrt{1-\exp\left(-\dfrac{\alpha_0^2}{u_{0\alpha}^2}\right)}} \sin^2(Q_\alpha \alpha_0)$$
$$\times \bar{S}(Q_\alpha)\delta(\omega_{0-}\pm \omega),$$

$$S(Q_\alpha, \omega)_{0-0-} = \frac{1}{1-\exp\left(-\dfrac{\alpha_0^2}{2u_{0\alpha}^2}\right)} \left|\left[\cos(Q_\alpha \alpha_0)\right.\right.$$
$$\left.\left.-\exp\left(-\dfrac{\alpha_0^2}{2u_{0\alpha}^2}\right)\right]\right|^2 \bar{S}(Q_\alpha)\delta(\omega), \quad (8)$$

with $\bar{S}(Q_\alpha) = \exp(-Q_\alpha^2 u_{0\alpha}^2)$. If $\alpha_0^2 \gg u_{0\alpha}^2$, this Gaussian profile is modulated by either $\cos^2(Q_\alpha \alpha_0)$ for $|0\pm\rangle \rightarrow |0\pm\rangle$ or $\sin^2(Q_\alpha \alpha_0)$ for $|0\pm\rangle \rightarrow |0\mp\rangle$. These terms arise because neutrons are scattered by the particle delocalized over both sites, either in-phase or out-of-phase. (Formally, the proton spin does not contribute to the interference mechanism.) This is analogous to double-slit experiments with electromagnetic waves. However, whereas in-phase and out-of-phase scattering are observed separately with electromagnetic waves, in the case of Eq. (8) the interference pattern is observed only if the tunnel splitting is greater than the energy resolution of the neutron-scattering experiments. Otherwise, summation of the $\cos^2(Q_\alpha \alpha_0)$ and $\sin^2(Q_\alpha \alpha_0)$ terms is a constant and only the Gaussian profile, free of quantum interference, corresponding to a simple harmonic oscillator is observed.

Interference fringes due to quantum entanglement can be thus clearly distinguished from those arising from other quantum effects. They were effectively observed for $KHCO_3$.[24]

For momentum transfer along x the analysis of the modulated profile gave $2x_0' = (0.64 \pm 0.06)$ Å. This is about the distance between the projections of the proton positions (1 and 2, in Fig. 1) onto the x axis. This distance is much

shorter than the separation of ≈ 2 Å between two protons in a dimer. This is direct evidence that interferences are related to proton dynamics, rather than to proton locations.

For momentum transfer along y, the analysis of the Q profile gave $2y_0' = (0.62 \pm 0.04)$ Å which corresponds to the shortest distance between projections of proton positions onto the y axis. However, these protons belong to different dimers in the unit cell (for example those labeled I and II in Fig. 1). Therefore spatially extended quantum correlation between dimers should occur.

Finally, interference for momentum transfer along z suggested that protons are slightly tilted perpendicular to the dimer mean plane and should be located at $\pm z_0' = \pm (0.25 \pm 0.02)$ Å. However, this is not visible in the crystal structure.

B. Vibrational decoupling

In hydrogen bonded systems, anharmonic coupling is normally regarded as an important mechanism mixing displacements of atoms into complex vibrational coordinates that are geodesics of the potential hypersurface depending on all atomic coordinates.[38,39] Within the framework of classical mechanics, each particle is univocally labeled and localized.

In the harmonic approximation, the dynamics of a dimer is represented with symmetric and antisymmetric normal coordinates (say $\{X_{is}, X_{ia}\}, i = 1, 2, \ldots, N$, where $2N$ is the number of degrees of freedom) that are linear combinations of atomic displacements. For $KDCO_3$ the wave function analogous to Eq. (3) is

$$\Xi_0(\cdots X_{ia}, X_{is} \cdots) = \prod_i^N \Psi_{0i}^a(X_{ia})\Psi_{0a}^s(X_{is} - \sqrt{2}X_{i0}'). \quad (9)$$

Here, the equilibrium positions for the dimer coordinates are at $\pm X_{i0}'$.

For $KHCO_3$, the wave function in the ground state should be antisymmetrical with respect to proton permutation and invariant for permutation of carbon and oxygen atoms that are bosons. Therefore direct quantization of the normal coordinates $\{X_{is}, X_{ia}\}$ gives a wave function analogous to Eq. (9) that violates the Pauli principle because indistinguishable fermions are in the same state. This is avoided if the set of atomic coordinates split into strictly independent subsets for indistinguishable fermions $\{x_{is}, x_{ia}\}$ on the one hand, and for bosons $\{X_{js}, X_{ja}\}$ on the other. Then, the wave functions Ψ_0 can be factored into wave functions Φ_0 for fermions and bosons, respectively. The wave function derived from Eqs. (5) and (9) is

$$\Xi_{0\pm}(\cdots x_{is}, x_{ia} \cdots X_{js}, X_{ja} \cdots)$$
$$= \prod_i \frac{1}{\sqrt{2}} \Phi_{i0}^a(x_{ia})[\Phi_{i0}^s(x_{is} - \sqrt{2}x_{i0}')$$
$$\pm \Phi_{i0}^s(x_{is} + \sqrt{2}x_{i0}')]$$
$$\times \prod_j \Phi_{j0}^a(X_{ja})\Phi_{j0}^s(X_{js} - \sqrt{2}X_{j0}'). \quad (10)$$

The decoupling of the protons from the lattice dynamics cancels the decoherence mechanism and, if there is no further decoherence process, quantum correlation can last for a long time. The spin-related decoupling of protons is more fundamental, and certainly more efficient, than any accidental or specially designed cancellation of coupling terms in the dynamical matrix. This separation is a prerequisite for observing quantum interferences arising from long-lived quantum entanglement.[23,24] Intuitively, the separation of atomic motions is primarily a consequence of the crystal symmetry (presumably the existence of centrosymmetric dimers is of central importance in the case of $KHCO_3$). We suspect this separation may be not caused by a significant gain of internal energy for an isolated dimer.

Among alternative decoherence mechanisms, spin-spin coupling can be ignored. In a dimer the distance between protons is ≈ 2 Å and spin-spin interaction is on the order of 10^4 Hz. Therefore quantum decoherence should occur on a time scale as long as $\approx 10^{-4}$ s.

C. Crystal of dimers

In the crystal, quantum entanglement within dimers "hides" the Fermionic nature of the protons. The singlet or triplet states obey the Bose-Einstein statistics and collective dynamics due to interdimer interaction are represented with phonons totally decoupled from the lattice dynamics. For the proton modes, the population of excited states is negligible at a low temperature. The ground states can be represented as $2Ag + Bg + 2Au + Bu$ symmetry species.[33] The g and u species correspond to collective oscillations of the singlet and triplet states, respectively. Recalling of the Fermionic nature of the protons, the ground state must be regarded as a superposition of coherent states with perfectly defined H-spin correlation throughout the crystal domain. Owing to the lack of an efficient decoherence mechanism via the lattice dynamics, the lifetime of the quantum coherence may be long enough to be probed with the elastic neutron-scattering technique.

The neutron-diffraction pattern anticipated for the dynamical structure of the sublattice of entangled protons is quite different from the Bragg peaks of the crystal lattice. The overall shape of the pattern depends on the dimensionality of the quantum correlation. Moreover, the pattern is not determined solely by the spatial distribution of entangled protons. It is also related to the proton dynamics and the symmetry of the phonon states imposes specific constraints to the phase of the scattered neutrons. Therefore a thorough analysis of both the spatial and dynamical structures of the proton sublattice is necessary to ensure that all necessary conditions for observing diffraction can be fulfilled.

Then, if this is the case, the diffraction pattern of entangled protons should be quite well separated from the Bragg peaks and, by analogy with the hydrogen molecule,[37] the intensity should be proportional to the total cross section for protons (≈ 80 barns). (In the absence of quantum correlation the contribution of H atoms to Bragg-peak intensities is proportional to the rather modest coherent scattering cross section—$\sigma_c \approx 1.76$ barns—while the intensity due to incoherent scattering is proportional to $\sigma_i \approx 80$ barns.) The dra-

matic enhancement of intensity offers a better chance for observing diffraction by entangled protons among the Bragg peaks.

Along the x direction of the $KHCO_3$ crystal, we can distinguish two subsets of dimeric entities (those labeled I or II, respectively, in Fig. 1). They are symmetrical with respect to the binary axis parallel to (a). Phonons for the singlet or triplet states correspond to symmetry species Bg and Bu, respectively. For elastic scattering with momentum transfer Q_x, neutrons are scattered coherently by lines of protons parallel to the y direction (see Fig. 1). These lines are arranged in a gratinglike structure composed of two subsets of pairs of parallel slits separated by $2x'_0$. The distance between equivalent pairs is $D_x \approx a/\cos 42° \approx 20.27$ Å. One subset of slits is shifted with respect to the other by $D_x/2$ and neutrons are scattered antiphase by the two subsets. The scattering function for coherent elastic scattering by this gratinglike structure can be written as

$$S(Q_x,\omega)_{0\tau0\tau}$$

$$= |\sum_j \langle \Theta_{x0\tau j}| [\exp iQ_x(x_{1j} - x'_0 j)$$

$$+ \exp iQ_x(x_{1j} + x'_0 j)] \exp ijQ_x D_x |\Theta_{x0\tau j}\rangle$$

$$+ \langle \Theta_{x0\tau j}| [\exp iQ_x(x_{2j} - x'_{0j})$$

$$+ \exp iQ_x(x_{2j} + x'_{0j})] \exp ijD_x |\Theta_{x0\tau j}\rangle - \langle \Theta_{x0\tau j'}|$$

$$\times [\exp iQ_x(x_{1j'} - x'_{0j'}) + \exp iQ_x(x_{1j'} + x'_{0j'})]$$

$$\times \exp ij'D_x |\Theta_{x0\tau j'}\rangle - \langle \Theta_{x0\tau j'}| [\exp iQ_x(x_{2j'} - x'_{0j'})$$

$$+ \exp iQ_x(x_{2j'} + x'_{0j'})] \exp ij'D_x |\Theta_{x0\tau j'}\rangle|^2, \qquad (11)$$

where j indexes the lattice sites and $j' = (j + \frac{1}{2})$.

For waves scattered by equivalent pairs, intensity is a maximum when $D_x/(2x'_0) = N_x$ is an integer number. Furthermore, constructive interference for waves scattered by the two subsets of double slits occurs when $D_x/(4x'_0) = N_x/2$ is half integer. All together, the intensity is a maximum when N_x is an odd integer number and $Q_x = \pm n_x 2\pi/(2x'_0)$, according to Eq. (7).

Similar lines of protons parallel to x can be seen in Fig. 1. They form a system of double slits separate by $2y'_0$. Phonons for the singlet and triplet states along y correspond to Ag and Au symmetry species, respectively. The distance between double slits is $D_y = b/2 \approx 2.81$ Å. Phase matching occurs if $N_y = b/(4y'_0)$ is an integer number, either odd or even. The intensity is a maximum at $Q_y = \pm n_y 2\pi/(2y'_0)$.

As the existence of double slits along z is not visible in the crystal structure, it is not necessary to pursue the phase matching condition for Q_z. The elastic coherent scattering function can be now expressed in a compact and general formula as

$$S_l(\mathbf{Q},\omega) = \prod_{i=1}^{l} \delta(Q_{\alpha i} \pm n_{\alpha i}\pi/\alpha'_{0i}) \prod_\alpha S_{0\alpha}(Q_\alpha,\omega);$$

$$l = 1 \text{ or } 2. \qquad (12)$$

If quantum coherence occurs in one dimension ($l=1$) diffraction should give rise to slabs of intensity perpendicular to the α_1^* direction in reciprocal space. The intensity should be a maximum at the center and should be depressed exponentially for increasing momentum transfer value perpendicular to α_1^*. If quantum coherence occurs in two dimensions ($l=2$) diffraction should give rods of intensity, perpendicular to the reciprocal plane (α_1^*, α_2^*). The intensity should decrease for increasing momentum transfer perpendicular to (α_1^*, α_2^*). Of course, coherence in three dimensions should give rise to peaks of intensity.

With the numerical values derived from previous experiments[24] and from crystal structure (see Table I), we estimate $N_x = 33 \pm 3$ and $N_y = 4.5 \pm 0.5$. These values are quite compatible with the phase matching conditions but, regarding error bars, it is not possible to conclude whether phase matching actually occurs or not. Direct observation of the diffraction pattern is presented in the next section.

IV. DIFFRACTION AND QUANTUM ENTANGLEMENT

With the single crystal diffractometer (SXD) at the ISIS pulsed neutron source[40] we have measured a rather large volume of the reciprocal space parallel to the (a^*,c^*) plane with single crystals ($\approx 3 \times 3 \times 2$ mm³) of KHCO₃ and KDCO₃ at 15 K (Figs. 3 and 4, respectively). Further analysis of the Bragg peaks is in accordance with the structure derived from the measurements performed at the reactor source (see Tables I–IV).

Compared to the four-circle diffractometer, the advantage of SXD is twofold. First, with the time-of-flight technique, the whole accessible range of reciprocal space is measured all at once for each neutron pulse. This is convenient for seeking signals in addition to the Bragg intensities. In contrast to this, with the four-circle technique, measurements were performed at the Bragg-peak positions, in order to obtain the best signal-to-noise ratio. Second, with the high flux of epithermal neutrons delivered by the spallation source, one can probe a much larger domain of reciprocal space than at a reactor source.

On the other hand, with the limited number of detectors available on SXD at the time of these measurements, only a limited sector of reciprocal space is measured for each crystal orientation. Figures 3 and 4 are concatenations of several crystal orientations corresponding to rotations by steps of $\approx 30°$ around a fixed axis. Measurements over the whole reciprocal space would require a number of different crystal orientations around different axes. With a four-circle instrument these crystal orientations are much more straightforward. In addition, with the time-of-flight technique each pixel in reciprocal space corresponds to a particular wave length. The data analysis is more complex than for monochromatic reactor-based neutron diffraction and it is not
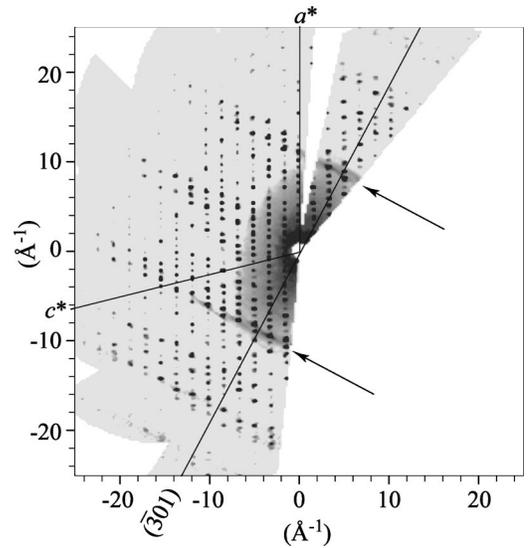

FIG. 3. Diffraction pattern of KHCO₃ at 15 K in the (a^*,c^*) plane. The arrows point to the ridges of intensity.

simple to account for the very large extinction coefficient of the KHCO₃ crystal (see Table I). In the present work, we have gained advantage from both techniques. The structure was determined at the best accuracy with the four-circles technique and quantum interference were quickly detected in the overview of the reciprocal space obtained with the time-of-flight technique.

In Figs. 3 and 4, the lines drawn along the ($\bar{3}01$) directions correspond to momentum transfer parallel to the dimer planes ($Q_y = Q_z = 0$). For KHCO₃, elastic and inelastic incoherent scattering give the broad signal centered at $\mathbf{Q} = 0$, which can be decomposed into a product of Gaussian-like profiles along and perpendicular to the ($\bar{3}01$) direction. The widths are roughly related to the inverse of the mean-squareamplitudes for the proton stretching (≈ 0.6
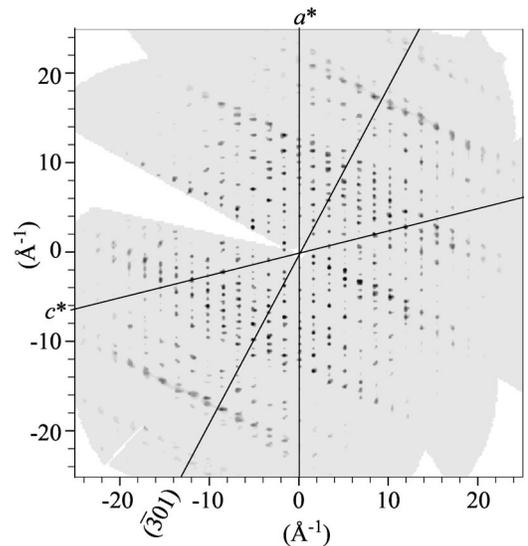

FIG. 4. Diffraction pattern of KDCO₃ at 15 K in the (a^*,c^*) plane.

$\times 10^{-2}$ Å^2) and out-of-plane bending ($\approx 2 \times 10^{-2}$ Å^2) modes, respectively. Quantum interference for proton pairs previously reported[24] is now hidden by inelastic scattering. (With the SXD instrument, scattered neutrons with different final energies are not distinguished.) Most of the central intensity due to incoherent scattering is no longer visible for the deuterated analog (Fig. 4).

For $KHCO_3$, the ridges of intensity perpendicular to the ($\bar{3}01$) direction observed at $\pm(10.25 \pm 0.25)$ Å^{-1} from the center (see arrows in Fig. 3) have all the characteristics anticipated for coherent scattering by entangled protons in planes containing the dimer entities (see below and Figs. 5–8): (i) the ridges are not due to coherent scattering by the whole lattice; (ii) they are not observed for the deuterated analog; (iii) they have rodlike shapes; (iv) orientations and positions are in accord with the structure of the proton sublattice. Additional ripples of diffuse scattering observed at $\approx \pm 17$ and ± 22 Å^{-1} for $KHCO_3$ are rather weak and broad (see Fig. 5) As they survive in the deuterated analog (see Fig. 6), they are not related to quantum statistics. They are tentatively attributed to thermal diffuse scattering (TDS).[30] These properties are further detailed below.

First, a cut of the map of intensity in the (a^*, c^*) plane parallel to a^* and at -4.50 Å^{-1} is totally free of Bragg peaks (Fig. 5). The sharp line at 9.25 Å^{-1} is the section of the ridge of intensity. The linewidth is similar to that of the Bragg peaks. This contrasts to the broad widths of TDS above 15 Å^{-1}.

Second, a similar cut for $KDCO_3$ confirms the absence of both the broad intensity due to incoherent scattering and the sharp ridge (Fig. 6). The TDS intensity at ≈ 20 Å^{-1} is the most intense ridge. This intensity should not depend on the isotope substitution. It can be used as a reference to compare relative intensities in Figs. 5 and 6. This comparison emphasizes the very weak TDS intensity compared to incoherent scattering. The weaker features between 5 and 20 Å^{-1} for $KDCO_3$ are also presumably due to TDS. They are largely hidden by incoherent scattering in $KHCO_3$.

Third, the profile observed along the ridge in the (a^*, c^*)

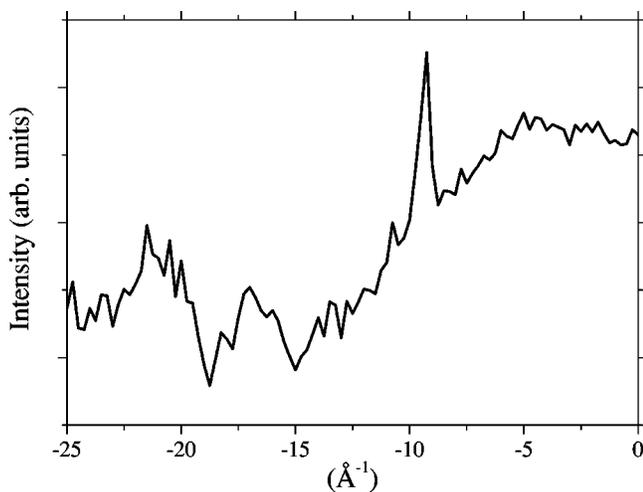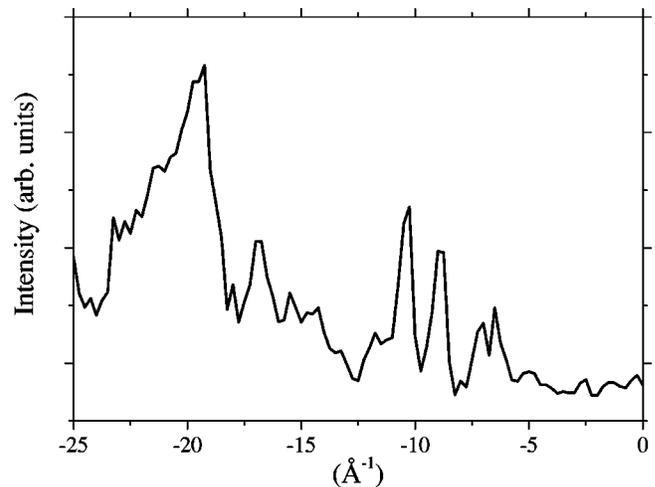FIG. 6. Cut of the diffraction pattern of $KDCO_3$ in the (a^*, c^*) plane along the line parallel to a^* and at -4.5 Å^{-1} from this axis.

plane (Fig. 7) is composed of sharp Bragg peaks superimposed on a Gaussian-like profile similar to that obtained for a cut, along the same direction, of the incoherent scattering signal centered at $\mathbf{Q}=0$. The maximum of intensity at ≈ 5 Å^{-1} corresponds to the intersection of the ridge with the ($\bar{3}01$) plane. This Gaussian-like profile demonstrates the absence of spatially extended quantum correlation perpendicular to the dimer plane.

Fourth, the ridge is still visible on the map of intensity for a slice of reciprocal space parallel to the (a^*, c^*) plane (7 pixels wide) shifted off by 7 pixels (≈ 0.5 Å^{-1}) along b^* (Fig. 8, A). The intensity of Bragg-peaks previously observed at $|\mathbf{Q}| \lesssim 10$ Å^{-1} is largely depressed. (The resolution of the SXD machine causes a few basal plane Bragg peaks at high $|\mathbf{Q}|$ to still be observed in this slice.) In contrast to this, the intensity of the Gaussian-like profile along the ridge is virtually unchanged [see the solid line with circles in Fig. 7
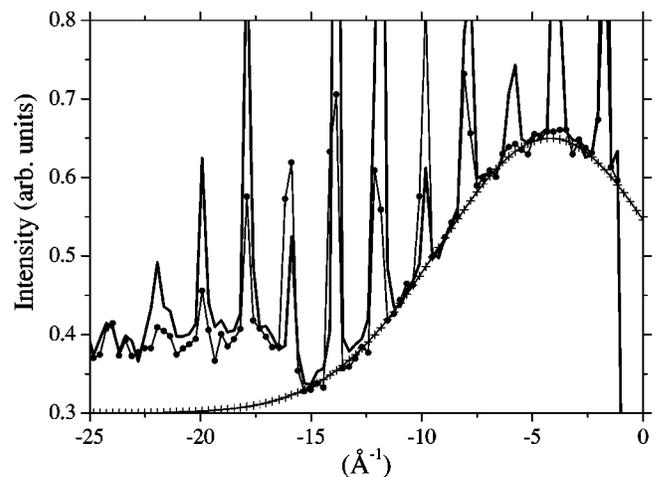

FIG. 5. Cut of the diffraction pattern of $KHCO_3$ in the (a^*, c^*) plane parallel to a^* and at -4.50 Å^{-1} from this axis.

FIG. 7. Cut of the diffraction pattern of $KHCO_3$ along the ridge of intensity (arrows in Fig. 3). Solid line: in the (a^*, c^*) plane. Thin line with circles ($-\bullet-$): 7 pixels (≈ 0.5 Å^{-1}) off the (a^*, c^*) plane. Crosses ($++++$): Gaussian profile for incoherent scattering shifted by -5 Å^{-1} for comparison.

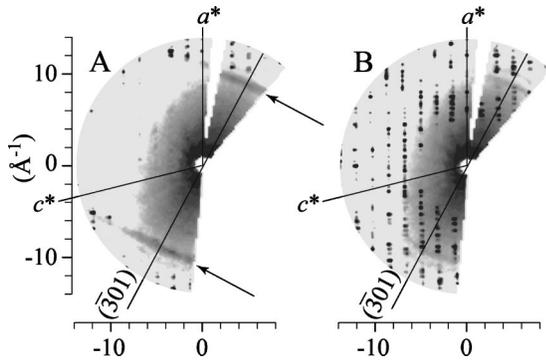FIG. 8. Cuts of the diffraction pattern of KHCO$_3$ parallel to the (a^*,c^*) plane. A: 7 pixels (≈ 0.5 Å^{-1}) off. B: 18 pixels (≈ 1.0 Å^{-1}) off.

for comparison with the profile in the (a^*,c^*) plane]. This is a further confirmation that the ridge and the Bragg reflections are quite different in nature.

Fifth, the ridge is no longer visible for the cut (9 pixels wide) shifted by 18 pixels (≈ 1.0 Å^{-1}) off the (a^*,c^*) plane while the broad incoherent scattering intensity at **Q** $=0$ is still very intense (Fig. 8, B). Therefore the width of the ridge perpendicular to the (a^*,c^*) plane is very much smaller than the width of the incoherent scattering signal along the same direction and diffraction by a sublattice of entangled protons in one dimension can be safely eliminated. On the other hand, the width perpendicular to the (a^*,c^*) plane (≈ 1 Å^{-1}) is similar to the width parallel to the same plane (see Fig. 5). This is in accordance with the rodlike shape anticipated for coherent scattering by a two-dimensional sublattice. It can be concluded that spatially extended quantum entanglement also occurs along the y direction, as anticipated from previous observation.[24] Further investigation of the reciprocal space should be necessary to observe the rods of intensity anticipated in the $(\bar{3}01)$ plane.

Finally, the intersection of the ridge with the $(\bar{3}01)$ direction is located at $Q_x = \pm (10.25 \pm 0.25)$ Å^{-1} from the center. This gives a separation of $2x'_0 = 2\pi/Q_x = (0.613 \pm 0.015)$ Å for the double slits. This is in perfect accordance with previous estimates and with the crystal structure. Furthermore, with the additional condition that N_x should be an odd integer number, the best estimate consistent with all observations is $N_x = 33$, $2x'_0 = 0.614$ Å, and $Q_x = \pm 10.23$ Å^{-1}. This solution is unique. The closest values $N_x = 31$ or 35 are not compatible with the crystal structure.

The real width of the ridge is related to the spatial extension of quantum coherence. Compared to the half width at half maximum (HWHM) of ≈ 6 Å^{-1} of the Gaussian-like profile for scattering by a single slit, the observed HWHM of ≈ 0.20 Å^{-1} (see Fig. 5) suggests that quantum coherence should extend itself over more than 30 double slits (more than 300 Å along the x direction). This is certainly an underestimate since the instrumental resolution ($\Delta|\mathbf{Q}|/|\mathbf{Q}| \approx 1\%$) is not negligible.

According to Eq. (11), another ridge of intensity is anticipated at $Q_x = \pm 4\pi/(2x'_0) = \pm (20.5 \pm 0.5)$ Å^{-1} from the

center. This should appear at ≈ 18 Å^{-1} in Fig. 5, but there is no conclusive signal in this region. Presumably, the intensity is dramatically depressed by the exponential factor in Eq. (11).

V. CONCLUSION

The Pauli principle and the dynamics of the centrosymmetric dimers in KHCO$_3$ impose quantum entanglement for the proton pairs. The ground state of each mode is a superposition of a singlet and a triplet state and strict separation of the proton dynamics from the other atoms occurs. The most effective decoherence mechanism is canceled out.

Collective dynamics of the singlet and triplet states are represented with phonons totally isolated from the lattice dynamics. These phonons belong to g and u symmetry species for the singlet and triplet states, respectively. Owing to the lack of decoherence mechanism, the dynamical structure arising from the long-lived spin correlation throughout the crystal can be probed with the elastic neutron-scattering technique.

Coherent scattering by the gratinglike structure of the sublattice of protons is observed with great intensity, quite separate from the Bragg peaks. The rodlike shape of the diffracted intensity demonstrates quantum correlation in two dimensions, parallel to the dimer planes. The absence of similar diffraction for the deuterated crystal emphasizes the role of quantum statistics.

KHCO$_3$ can be termed a "quantal crystal" (or Q'stal). The superposition of fully entangled macroscopic vibrational states with long lifetime is a dramatic burst of the quantum paradoxes into the macroscopic world. The quantum character is clearly observed at 15 K, which is quite a high temperature compared to normal operation of superconducting devices. Transition from quantal to classical crystal is anticipated to occur at sufficiently high temperature. If the main decoherence mechanism is the occurrence of proton disorder monitored by the known asymmetrical double minimum potential with an energy difference $\Delta E = 216$ cm^{-1} or 324 K between the two wells,[29] the Q'stal could survive rather close to room temperature.

If our interpretation, based upon the Pauli principle for centrosymmetric hydrogen bonded dimers, is correct, superpositions of macroscopic quantum states should occur in similar systems. This is in line with the interconversion mechanism of benzoic acid dimers in the solid state.[22] In that case, it has been reported that quantum coherence increases upon excitation of a particular phonon.

Quantum coherence in KHCO$_3$ is apparently quite at variance with the decoherence-free noiseless molecular subsystems in solution, demonstrated with NMR techniques, that could be used as quantum computer.[41–44] However, our finding that decoherence can be naturally canceled by properly chosen crystal symmetry and quantum statistics could be of some consequence to further protection against noise of quantum information storage and processing.

Compared to superconductivity and superfluidity, the KHCO$_3$ Q'stal shows some remarkable similarities, such as entangled pairs of fermions and large-scale long-lived quan-

tum coherence in the ground state. The superposition of macroscopic quantum states is also comparable to the current states in SQUID experiments. Indeed, these similarities are natural consequences of the basic principles of quantum physics. At the same time, the Q'stal is quite different from other macroscopic quantum systems. The entangled pairs are not mobile, they are totally decoupled from the host lattice and the quantum coherence could survive at rather high temperature. This state of the matter deserves further investigations.

---

*Electronic address: fillaux@glvt-cnrs.fr

[1] A. Einstein, B. Podolsky, and N. Rosen, Phys. Rev. **47**, 777 (1935).

[2] C.A. Kocher and E.D. Commins, Phys. Rev. Lett. **18**, 575 (1967).

[3] S.J. Freedman and J.F. Clauser, Phys. Rev. Lett. **28**, 938 (1972).

[4] A. Aspect, P. Grangier, and G. Roger, Phys. Rev. Lett. **47**, 460 (1981).

[5] J.S. Bell, Physics (Long Island City, N.Y.) **1**, 195 (1964).

[6] M.G. Moore and P. Meystre, Phys. Rev. Lett. **85**, 5026 (2000).

[7] E. Hagley, X. Maître, G. Nogues, C. Wunderlich, M. Brune, J.M. Raimond, and S. Haroche, Phys. Rev. Lett. **79**, 1 (1997).

[8] H. Pu and P. Meystre, Phys. Rev. Lett. **85**, 3987 (2000).

[9] L.-M. Duan, A. Sørensen, J.I. Cirac, and P. Zoller, Phys. Rev. Lett. **85**, 3991 (2000).

[10] D. Bouwmeester, Nature (London) **390**, 575 (1997).

[11] E.J. Brändas and C.A. Chatzidimitriou-Dreismann, Lect. Notes Phys. **325**, 485 (1989).

[12] C. A. Chatzidimitriou-Dreismann, Adv. Chem. Phys. **99**, 393 (1997).

[13] C.A. Chatzidimitriou-Dreismann, T.A. Redah, R.M.F. Streffer, and J. Mayers, Phys. Rev. Lett. **79**, 2839 (1997).

[14] E.B. Karlsson, C.A. Chatzidimitriou-Dreismann, T. Abdul-Redah, R.M.F. Streffer, B. Hjörvarsson, J. Öhrmalm, and J. Mayers, Europhys. Lett. **46**, 617 (1999).

[15] E.B. Karlsson and S.W. Lovesey, Phys. Rev. A **61**, 062714 (2000).

[16] E.B. Karlsson and S.W. Lovesey, Phys. Scr. **65**, 112, 118 (2002).

[17] S. Habib, K. Shizume, and W.H. Zurek, Phys. Rev. Lett. **80**, 4361 (1998).

[18] L. Viola, E. Knill, and S. Lloyd, Phys. Rev. Lett. **82**, 2417 (1999).

[19] T. Calarco, M. Cini, and R. Onofrio, Europhys. Lett. **47**, 407 (1999).

[20] A.O. Caldeira and A.J. Leggett, Ann. Phys. (N.Y.) **149**, 374 (1983).

[21] J.R. Friedman, V.P.W. Chen, S.K. Tolpygo, and J.E. Lukens, Nature (London) **406**, 43 (2000).

[22] F. Fillaux, M.-H. Limage, and F. Romain, Chem. Phys. **276**, 181 (2002).

[23] F. Fillaux, Physica D **113**, 172 (1998).

[24] S. Ikeda and F. Fillaux, Phys. Rev. B **59**, 4134 (1999).

[25] www.isis.rl.ac.uk/excitation/mari.

[26] www-llb.cea.fr.

[27] J.O. Thomas, R. Tellegren, and I. Olovsson, Acta Crystallogr., Sect. B: Struct. Crystallogr. Cryst. Chem. **30**, 1155 (1974).

[28] J.O. Thomas, R. Tellegren, and I. Olovsson, Acta Crystallogr., Sect. B: Struct. Crystallogr. Cryst. Chem. **30**, 2540 (1974).

[29] F. Fillaux, Chem. Phys. **74**, 405 (1983).

[30] C. C. Wilson, *Single Crystal Neutron Diffraction from Molecular Materials*, Series on Neutron Techniques and Applications, edited by J.L. Finney and D.L. Worcester, Vol. 2 (World Scientific Co. Pte. Ltd., Singapore, 2002).

[31] A. Novak, P. Saumagne, and L.D.C. Bock, J. Chim. Phys. Phys.-Chim. Biol. **60**, 1385 (1963).

[32] K. Nakamoto, Y.A. Sarma, and K. Ogoshi, J. Chem. Phys. **43**, 1177 (1965).

[33] G. Lucazeau and A. Novak, J. Raman Spectrosc. **1**, 573 (1973).

[34] F. Fillaux, J. Tomkinson, and J. Penfold, Chem. Phys. **124**, 425 (1988).

[35] S. Kahsida, S. Ikeda, and Y. Nakai, J. Phys. Soc. Jpn. **63**, 4643 (1994).

[36] C. Cohen-Tannoudji, B. Diu, and F. Laloë, *Mécanique Quantique* (Hermann, Paris, 1977).

[37] S. W. Lovesey, *Nuclear Scattering, Theory of Neutron Scattered from Condensed Matter* (Clarendon, Oxford, 1984).

[38] A. Novak, Struct. Bonding (Berlin) **18**, 177 (1974).

[39] P. Schuster, G. Zundel, and C. Sandorfy, *The Hydrogen Bond: Recent Developments in Theory and Experiments* (North-Holland Pub. Co., Amsterdam, New York, 1976).

[40] www.isis.rl.ac.uk/crystallography.

[41] E.M. Fortunato, M.A. Pravia, N. Boulant, G. Teklemarian, T.F. Havel, and D.G. Cory, J. Chem. Phys. **116**, 7599 (2002).

[42] A. Galindo and M.A. Martin-Delgado, Rev. Mod. Phys. **74**, 347 (2002).

[43] E.M. Fortunato, L. Viola, J. Hodges, G. Teklemarian, and D.G. Cory, New J. Phys. **4**, 5.1 (2002).

[44] G. Teklemarian, E.M. Fortunato, M.A. Pravia, T.F. Havel, and D.G. Cory, Chaos, Solitons Fractals **16**, 457 (2003).